

## Long time interaction of envelope solitons and freak wave formations

Didier Clamond<sup>a,c,\*</sup>, Marc Francius<sup>b,d</sup>, John Grue<sup>c</sup>, Christian Kharif<sup>d</sup>

<sup>a</sup> *Institutt For Energiteknikk, P.O. Box 40, 2027 Kjeller, Norway*

<sup>b</sup> *TNO Defense, Safety and Security, Electro-Optics Group, P.O. Box 96864, 2509 JG The Hague, The Netherlands*

<sup>c</sup> *Mechanics Division, Department of Mathematics, University of Oslo, P.O. Box 1053 Blindern, 0316 Oslo, Norway*

<sup>d</sup> *Institut de Recherche sur les Phénomènes Hors Équilibre, 49 Rue Frédéric Joliot-Curie, B.P. 146, 13384 Marseille, France*

Received 31 October 2005; received in revised form 18 February 2006; accepted 20 February 2006

Available online 5 June 2006

---

### Abstract

This paper concerns long time interaction of envelope solitary gravity waves propagating at the surface of a two-dimensional deep fluid in potential flow. Fully nonlinear numerical simulations show how an initially long wave group slowly splits into a number of solitary wave groups. In the example presented, three large wave events are formed during the evolution. They occur during a time scale that is beyond the time range of validity of simplified equations like the nonlinear Schrödinger (NLS) equation or modifications of this equation. A Fourier analysis shows that these large wave events are caused by significant transfer to side-band modes of the carrier waves. Temporary downshiftings of the dominant wavenumber of the spectrum coincide with the formation large wave events. The wave slope at maximal amplifications is about three times higher than the initial wave slope. The results show how interacting solitary wave groups that emerge from a long wave packet can produce freak wave events.

Our reference numerical simulation are performed with the fully nonlinear model of Clamond and Grue [D. Clamond, J. Grue, A fast method for fully nonlinear water wave computations, *J. Fluid Mech.* 447 (2001) 337–355]. The results of this model are compared with that of two weakly nonlinear models, the NLS equation and its higher-order extension derived by Trulsen et al. [K. Trulsen, I. Kliakhandler, K.B. Dysthe, M.G. Velarde, On weakly nonlinear modulation of waves on deep water, *Phys. Fluids* 12 (10) (2000) 2432–2437]. They are also compared with the results obtained with a high-order spectral method (HOSM) based on the formulation of West et al. [B.J. West, K.A. Brueckner, R.S. Janda, A method of studying nonlinear random field of surface gravity waves by direct numerical simulation, *J. Geophys. Res.* 92 (C11) (1987) 11 803–11 824]. An important issue concerning the representation and the treatment of the vertical velocity in the HOSM formulation is highlighted here for the study of long-time evolutions.

© 2006 Elsevier SAS. All rights reserved.

---

\* Corresponding author.

*E-mail addresses:* [didier.clamond@ife.no](mailto:didier.clamond@ife.no) (D. Clamond), [marc.francius@tno.nl](mailto:marc.francius@tno.nl) (M. Francius), [johng@math.uio.no](mailto:johng@math.uio.no) (J. Grue), [kharif@irphe.univ-mrs.fr](mailto:kharif@irphe.univ-mrs.fr) (C. Kharif).

## 1. Introduction

In recent years, an increasing number of damages due to collision of giant waves with ships or platforms has been reported. These giant waves, also called freak waves or rogue waves, represent extreme wave events during which a short group of extremely large waves occurs with elevations exceeding the average elevation of the surrounding wave field by a factor two or more. A recent review on observations of these giant waves and on the various physical mechanisms leading to their formation can be found in [4].

Among the various mechanisms that have been proposed to explain the occurrence of freak waves in deep water and in the absence of currents, the spatio-temporal dispersive focusing of wave packets and the nonlinear self-focusing of a continuous wave train are the most popular ones to describe the focusing of wave energy over a small area of the wave field. In the nonlinear self-focusing mechanism, the focusing of the wave energy results from the evolution of intrinsic instabilities of nonlinear uniform wave trains subject, initially, to slowly modulated periodic (side-band) disturbances. The evolution of this type of instability, which is also known as the Benjamin–Feir or modulational instability, has been extensively studied and is well-known [5–7]. Recent studies on the modulational instability of a uniform wavetrain have shown that many features of the observed freak waves are consistent with certain analytic breather-type solutions of the much celebrated nonlinear Schrödinger (NLS) equation [8–10]. In contrast, the spatio-temporal dispersive focusing mechanism does not require the presence of a uniform wavetrain to explain the formation of freak waves. This mechanism has been studied in [11] for deep water waves in the framework of the NLS equation. It has been shown that pure dispersion effects can produce freak waves during the evolution of a localized wave packet, but only when there is initially a specific spatial distribution of frequencies in the wave packet (chirped frequency modulation). It has also been shown in [11] that the effects of frequency modulation can affect significantly the development of the Benjamin–Feir instability of a weakly nonlinear modulated wavetrain, in particular when the initial amplitude of the wave train is small.

In this paper, we study numerically the long time evolution of a wave packet in deep water with small initial steepness and without initial frequency modulation. This initial-value problem is well known and has been much studied experimentally and theoretically. Applying the inverse scattering technique to the NLS equation, Zakharov and Shabat [12] solved this initial value problem to obtain predictions on the asymptotic behavior of the wave group when the initial steepness is small. Their solution predicts that an envelope pulse, whatever the exact shape of its amplitude modulation, evolves eventually into a finite number of envelope solitons plus a small dispersive decaying wave group. As far as the number of formed solitary wave groups is of interest, the agreement between theory and experiment is good if the initial steepness is sufficiently small [7,13]. For large enough initial steepness or long enough wave packets the theoretical predictions of formed solitons deviate more from observations. The most striking observations are strong asymmetric modulations in the envelope of the wave packets during the group splitting and frequency downshift in the leading groups.

Detailed comparisons of numerical results based on NLS equation with experiments in a wave tank, carried out in [14], have demonstrated that this equation can describe only the beginning of the transformation process before any significant effects contribute to the asymmetry in the wave group envelope. A better correspondence between numerical results and experiments in a long wave tank has been reported in [15] using a spatial version of the Dysthe model, which is an higher-order extension of NLS equation as derived by Dysthe in [16]. In fact, these two approximate models are limited to weakly nonlinear waves and narrow-banded spectra. When nonlinear energy focusing at the center of the group occurs, there is a significant widening of the spectrum and the models' assumptions may be violated. This, in turn, affects the accuracy and the validity for long-time simulations. A less restrictive alternative for weakly nonlinear wave field is to employ the well-known Zakharov's equation based on the Hamiltonian formalism, because it has no restrictions on the spectral width. It is accurate to the third order in wave steepness. A spatial version of the Zakharov model should be used in order to describe the spatial evolution of wave groups along a wave tank. Recently in [17], experimental results have been compared with numerical results obtained from a spatial version of the Zakharov equation derived in [18]. Furthermore, the validity of the Dysthe model (spatial version) is tested against experiments and the Zakharov's model predictions. For rather short periodic wave groups a very good agreement has been obtained between the experimental results and the simulations based on both Zakharov and Dysthe models for various initial shapes, amplitudes and spectral contents. However, the performance of these models have not been tested for rather long wave groups.

The main purpose of this study is to describe how an initially long waves packet splits into a number of solitary wave groups, and how large wave events are formed during the split-up process. This kind of behavior has been presented in [19], and it has been suggested that the interaction between solitary wave groups is a source of freak wave formations. During the split-up process, three large wave events occur before the separation of the leading group. Ultimately, the group of waves evolves into three solitary wave groups, which separate because each one propagates with a different velocity although each has the same carrier wavenumber (as in the initial wave group). In this study we re-examine this scenario using two different fully nonlinear formulations. The fully nonlinear results are in a good agreement and exhibit a different scenario than that based on predictions of NLS equation and an extended version of the Dysthe equation as derived in [2].

The paper is organized as follows. In Section 2, we describe briefly the models we used, as well as the numerical experiment which is considered. The long time behavior of the evolution of the wave group and the comparison between the different models are analyzed in Section 3. Some local phenomena occurring during the formation of freak waves are analyzed in Section 4. Finally, in Section 5, we discuss the occurrence of multiple collisions between solitary wave groups and their relation with freak wave formation. In Section 6, conclusions are drawn.

## 2. Numerical models and experiment

In order to study the dynamics of a long wave packets and the subsequent group splitting for long time evolution, we use a fully nonlinear model for deep water gravity waves which accounts for all strong nonlinear features of the (non-breaking) wave group dynamics. We use the fast and accurate model developed by Clamond and Grue [1]; this fully nonlinear model will be referred as CG for brevity. In the following, the model is briefly described as well as the other numerical models, which are also used for comparison with the CG results. All the models are run using the same initial condition described in the last sub-section.

### 2.1. Fully nonlinear model

We consider two-dimensional surface gravity wave motions in deep water and potential flow. Let  $x$ ,  $y$ ,  $t$  be the horizontal, upward vertical and time variables, and let  $\eta(x, t)$  be the surface elevation relative to the mean level  $y = 0$ . Let also  $\phi$  and  $\psi$  be the velocity potential and the stream function, respectively, that are linked by the Cauchy–Riemann relations,  $\phi_x = \psi_y$ ,  $\phi_y = -\psi_x$ . The functions  $\psi$  and  $\phi_y$  decay to zero for  $y \rightarrow -\infty$ , the surface impermeability and zero pressure conditions read

$$\eta_t + \tilde{\psi}_x = 0, \quad (1)$$

$$\tilde{\phi}_t + g\eta + \frac{\tilde{\phi}_x^2 - \tilde{\psi}_x^2 + 2\eta_x \tilde{\phi}_x \tilde{\psi}_x}{2(1 + \eta_x^2)} = 0, \quad (2)$$

where the ‘tildes’ denote the functions at  $y = \eta$ . These relations provide two prognostic equations to update at instant  $t + \Delta t$  the surface  $\eta$  and the potential at the surface  $\tilde{\phi}$  from their values at instant  $t$ .

To complete the system, one must solve the Cauchy–Riemann relations in order to update  $\tilde{\psi}$ . This is achieved via the Cauchy integral formula. The real part of this Cauchy integral formula yields

$$\tilde{\phi} = \frac{1}{\pi} \int_{-\infty}^{\infty} \frac{D(\tilde{\phi}' - \eta'_x \tilde{\psi}') - \tilde{\psi}' - \eta'_x \tilde{\phi}'}{1 + D^2} \frac{dx'}{x' - x}, \quad (3)$$

where  $D = (\eta' - \eta)/(x' - x)$ ,  $\tilde{\phi} = \tilde{\phi}(x, t)$ ,  $\tilde{\phi}' = \tilde{\phi}(x', t)$ , etc. After some simple rearrangements (see [1] for details), this relation yields

$$\begin{aligned} \tilde{\psi}_x = & \mathcal{H}\{\tilde{\phi}_x\} + \partial_x \{\eta \tilde{\phi}_x\} + \partial_x \{\mathcal{H}\{\eta \mathcal{H}\{\tilde{\phi}_x\}\}\} + \mathcal{H}\left\{ \frac{1}{\pi} \int_{-\infty}^{\infty} \frac{D^2(D - \eta_x) \tilde{\phi}'_x}{1 + D^2} \frac{dx'}{x' - x} \right\} \\ & - \mathcal{H}\left\{ \frac{1}{\pi} \int_{-\infty}^{\infty} \frac{D(D - \eta_x) \tilde{\psi}'_x}{1 + D^2} \frac{dx'}{x' - x} \right\}, \end{aligned} \quad (4)$$

where  $\mathcal{H}\{f\} = f_{-\infty}^{\infty} \frac{f(x')}{x'-x} \frac{dx'}{\pi}$  is the Hilbert transform.

The three first terms in the right-hand side of (4) are convolution products and are therefore computed very quickly via fast Fourier transforms. The two last terms involve integrals with rapidly decaying kernels, they can thus be computed quickly and accurately truncating the integration over a limited region (here, one wavelength). Hence, the evaluation of  $\tilde{\psi}_x$  requires  $O(N_c \times N_w)$  operations,  $N_c$  the total number of computational nodes and  $N_w$  the number of nodes per wavelength.  $N_w \ll N_c$  for large domains and the computation of the integrals is easily parallelizable. It turns out that, for the experiment described below, the practical computational cost is close to  $O(N_c \times \log N_c)$  operations per time step. Indeed, for this peculiar experiment, we found that integrations over one wavelength in front and back (so two wavelengths in total) and that two iterations were needed. Longer integrations and more iterations did not give different results.

For the time stepping, the linear part of the system (1), (2) is integrated analytically, thus allowing larger time steps and providing a linearly unconditionally stable and exact scheme. For the nonlinear remaining part, we use a eighth-order Runge–Kutta scheme with an auto-adapting time step.

To test the method, we simulated the propagation over 1000 periods of the pure Stokes wave with the numerical parameters given in Section 2.4. After 1000 periods, the phase shift error is  $23^\circ$  and the relative error on the energy is about  $10^{-5}$ . This test clearly illustrates the accuracy of the numerical model. The numerical procedure in the three-dimensional implementation is documented and tested in details in [1]; further convincing tests are given in [20–23].

## 2.2. High-order spectral method

To support the predictions obtained in [19] with the CG model, we have also implemented a high-order spectral method (HOSM) slightly different than that proposed by West et al. [3] and Dommermuth and Yue [24]. In these methods, the conjugate Hamiltonian equations (1), (2) are rewritten

$$\eta_t + \tilde{\phi}_x \eta_x - (1 + \eta_x^2)W = 0, \quad (5)$$

$$\tilde{\phi}_t + g\eta + \frac{1}{2}\tilde{\phi}_x^2 - \frac{1}{2}(1 + \eta_x^2)W^2 = 0, \quad (6)$$

where  $W = \tilde{\phi}_y$  is the vertical velocity at the surface that is determined solving approximately a Laplace equation for given  $\eta$  and  $\tilde{\phi}$ . This approximation is obtained up to an arbitrary order  $M$  in wave steepness, using a Taylor series expansion technique and assuming the convergence of the series expansions of  $\tilde{\phi}_y$  and  $\tilde{\phi}$ . As explained by Tanaka [25], there exists an important difference between the two original versions of HOSM, concerning the series for  $\tilde{\phi}_y$ . In fact, the version of West et al. differs from the version of Dommermuth and Yue not only in the expression of the approximated vertical velocity at the surface, but also in its subsequent treatment in the free surface equations. According to West et al. [3], the surface equations must be truncated at consistent nonlinear order if they are to simulate a conservative Hamiltonian system. This requires to treat carefully all nonlinear terms containing  $W$  in the prognostic equations. In contrast to the series used by Dommermuth and Yue, those used by West et al. are naturally ordered with respect to the nonlinear parameter  $\epsilon$ , which is a measure of the wave steepness. Thus, the Dommermuth and Yue formulation is not consistent, after truncation, with the underlying Hamiltonian structure of the canonical pair of free-surface equations. In this paper, we have used the West et al. version which preserves the Hamiltonian structure of the prognostic equations, although the free surface equations are advanced in time explicitly using a fourth-order Runge–Kutta integrator as in Dommermuth and Yue [24].

The accuracy of the HOSM method has been tested towards reference computations of Stokes waves in [3,24,26]. It was reported that for Stokes wave with steepness  $ak > 0.3$ , the expected rate of convergence of the perturbation series in the HOSM is not realized by increasing the order parameter  $M$ . In general, the number of points in the numerical method must be sufficiently large for this convergence to occur. This means that when the local steepness increases up to 0.3 or higher values, the HOSM should perform less well in these regions. In order to eliminate high-wave number instabilities that can severely limit the HOSM, we have applied at each time step an ideal low-pass filter to  $\eta$  and  $\tilde{\phi}$  of the form

$$F(k) = \begin{cases} 1 & \text{if } |k| < k_{\max}, \\ 0 & \text{if } |k| > k_{\max}, \end{cases} \quad (7)$$

where  $k_{\max}$  is the highest wavenumber in the amplitude spectrum. Because of aliasing errors, this technique limits the number of alias-free modes that are effectively resolved in the numerical simulation. Nevertheless, we have checked in our numerical experiments that this smoothing technique has no significant effect on the evolution of the wave field, provided  $k_{\max}$  is sufficiently large.

### 2.3. Schrödinger and Dysthe models

Under the assumptions of small amplitudes, narrow banded spectra and propagation in one direction, various simplified equations can be derived. Two prominent examples are the well-known nonlinear Schrödinger equation (NLS) and Dysthe's equation. These models have been widely used to confirm the Benjamin–Feir instability mechanism. For long time simulations of one dimensional, weakly modulated weakly nonlinear wavetrain, it has been suggested that NLS is a sufficiently accurate model when the initial steepness is small, independently of the number of waves in the modulation [8]. In this study, we have also implemented two weakly nonlinear models in order to test their validity in the long-time simulation of nonlinear wave groups.

The simplest model is the classical nonlinear Schrödinger equation written for the complex envelope  $A(x, t)$  of the elevation  $\eta(x, t) = \text{Re}\{A(x, t) e^{i(k_0 x - \omega_0 t)}\}$ , as

$$A_t + c_g A_x + \frac{i}{4} c_g k_0^{-1} A_{xx} + \frac{i}{2} \omega_0 k_0^2 |A|^2 A = 0, \quad (8)$$

where  $c_g = \omega_0/2k_0$  is the linear group velocity. This equation admits the envelope soliton solution

$$A = a_1 \text{sech}[\sqrt{2} a_1 k_0^2 (x - c_g t)] e^{-i a_1^2 k_0^2 \omega_0 t / 4}. \quad (9)$$

The NLS equation admits other analytical solutions, for instance with oscillating envelope. One of these solutions is described and used in Section 4.

We have used a more accurate model, an extended Dysthe equation (EDE) derived in [2], which accounts for fourth-order effects in the envelope equation. This EDE envelope equation follows as

$$A_t + \mathcal{F}^{-1} \left\{ (\omega - \omega_0) \mathcal{F}\{A\} \right\} + \frac{i}{2} \omega_0 k_0^2 |A|^2 A + \frac{3}{2} \omega_0 k_0 |A|^2 A_x - \frac{1}{4} \omega_0 k_0 A^2 A_x^* + \frac{i}{2} \omega_0 k_0 A \mathcal{H}\{|A|^2\}_x = 0, \quad (10)$$

where  $\mathcal{F}$  and  $\mathcal{H}$  are the Fourier and Hilbert transforms. As explained in [2], the EDE equation is an heuristic model that has improved bandwidth resolution and improved stability properties, in contrast with the classical Dysthe equation and a higher-order extension of NLS equation derived in [27] with a broader bandwidth assumption  $\mu = O(\varepsilon_0^{1/2})$ . Usually,  $\mu = \Delta k/k_0$  is the frequency dispersion parameter where  $\Delta k$  is the spectral bandwidth, and  $\varepsilon_0 = a k_0$  is the nonlinearity parameter. In terms of these two parameters, the narrow-band assumption employed to derive the NLS equation and the classical Dysthe equation is enforced with the relation  $\mu = O(\varepsilon_0)$  for both equations. As demonstrated in [28], employing appropriate bandwidth constraints on both the linear and nonlinear parts of the third-order Zakharov equation leads to both the NLS equation and the classical Dysthe equation. Thus, the EDE equation can be seen as a limiting case of the Zakharov integral equation after considering an appropriate limit on the spectral width only for the cubic nonlinear part. Given that the EDE equation captures the full linear dispersion behavior, this model is exact in the linear limit. Nevertheless, these models are, a priori, valid for relatively short term simulations; NLS is valid for dimensionless times  $t/T_0 = O(\varepsilon_0^{-2})$  where  $T_0$  is the period of the carrier wave, while the EDE model is valid for  $t/T_0 = O(\varepsilon_0^{-3})$ .

### 2.4. Initial condition

The initial state of the wave field is specified in two steps. First an exact steady Stokes wave [29], with wavenumber  $k_0$  and amplitude  $a_0$  is computed ( $a_0$  is half the total wave height and  $\varepsilon_0 \equiv k_0 a_0$  is the initial steepness). Secondly, the surface elevation and the tangential velocity at the surface are multiplied by the bell function  $\text{sech}[\hat{\varepsilon} \sqrt{2} a_0 k_0^2 (x - x_0)]$  where the parameter  $\hat{\varepsilon}$  determines the length of the wave packet. An exact soliton solution of the nonlinear Schrödinger equation is obtained with  $\hat{\varepsilon} = 1$  (see Eq. (9)). An initial condition with  $\varepsilon_0 = 0.09$  and  $\hat{\varepsilon} = 0.26$  are input to the different nonlinear numerical models presented above. The computational domain involves 128 carrier wavelengths. The carrier wave is discretized over 32 nodes per wavelength. This means that all harmonics up to the 15th are resolved with the CG model, and that 128 Fourier modes are included in the spectral band  $[k_0 - \frac{1}{2}k_0; k_0 + \frac{1}{2}k_0]$ .

## 2.5. Remarks

As suggested by one of the referees on this paper, an alternative way to support the CG predictions would have been to use the recent method of direct numerical solution of Euler equation, describing potential oscillations of ideal fluid with a free surface in a gravitational field. This solution was recently used, for instance in [30], to simulate freak waves generated by the nonlinear development of the modulational instability of Stokes's waves. This method is based on conformal mapping and no approximations are made.

It is well-known that methods based on conformal mapping can suffer very severe drawbacks when extreme waves occur. To avoid these limitations, a huge number of nodes is usually required. We add that using a huge number of nodes per wavelength (assuming that the Fourier series converge) induces a large accumulation of round-off errors, thus limiting the gain that one can expect. Hence, even for short domains, the accuracy of simulations of steep waves based on conformal mapping may be questionable.

In view of the length of our numerical domain and the number of waves in the initial wave packet, it might be that these methods are computationally more expensive than the fully nonlinear methods used in this study (for the same accuracy), in order to study the long time evolution and focusing of long wave groups with the occurrence of many freak waves events.

## 3. Long time evolution

We first consider the global picture of the evolution of the surface elevation  $\eta$ , as predicted by the (fully nonlinear) CG model (see Fig. 1). According to this model, three large wave events occur during the 3000 wave periods of simulation. The first large wave event occurs after  $t/T_0 = 155$ ; then  $k_0\eta_{\max} = 0.2866$  ( $k\eta_{\max} = 0.34$ ,  $k$  the local wavenumber) which is the maximal wave elevation observed during the computations. The second large wave event occurs after  $t/T_0 = 410$ ; then  $k_0\eta_{\max} = 0.2545$ . The third large wave event occurs after  $t/T_0 = 627$ ; then  $k_0\eta_{\max} = 0.2704$ .

At about  $t/T_0 \simeq 1200$ , the wave field consists of three separated solitary wave groups with ordered heights, the steepest being ahead. The fundamental wavenumber of each group is  $k_0$ . Up to 3000 wave periods (and after) the groups separate slowly, each group traveling with its characteristic speed. We have compared the shape of each (well separated) solitary wave group (at  $t/T_0 = 3000$ ) with the analytical envelope soliton solution of NLS (9). For each (separated) envelope soliton there is a fairly good agreement with the analytical NLS solutions as far as the wave envelope is of interest (this is not shown here). This suggests that the observed wave dynamics can be explained as nonlinear interactions between three perturbed NLS solutions. Nevertheless, it should be noted that the speed of each solitary wave group is not equal to the linear group velocity, as predicted by the NLS theory. The leading two solitary wave groups move faster than the linear group velocity, while the trailing small solitary group moves slower than the linear group velocity.

### 3.1. Comparison with Schrödinger and Dysthe equations

The results obtained with the weakly nonlinear models presented in Section 2.3 are compared with the fully nonlinear computations. Fig. 2 illustrates the differences between the weakly nonlinear models and the CG model for the envelope dynamics. It also shows snapshots from the evolution of the wave envelope and how the initial group splits into three solitons according to the CG model. The smallest soliton in the trailing portion of the wave group is the first to detach from the wave group. The fully nonlinear model predicts two interacting solitary envelopes in the leading part of the wave train. It is evident that the fully nonlinear solutions obtained using CG and the weakly nonlinear NLS or EDE, apart from times up to  $t/T_0 = 100$  and  $t/T_0 = 300$ , respectively, describe different long-time evolutions. The analytical theory of the NLS equation predicts that any symmetric shape envelope (with uniform wavenumber or frequency within the group) disintegrates into a finite number of solitons which propagate with the same speed, the linear group velocity, and a small oscillatory tail. Thus, for our initial condition, it predicts the formation of three solitons that are attached to each other. Furthermore, the corresponding envelope always remains symmetric with respect to the center of the wave group. These bound-solitons describe very mild modulations of the envelope amplitude (very long period of recurrence). Although the NLS equation fails to predict the wave dynamics beyond its time range of

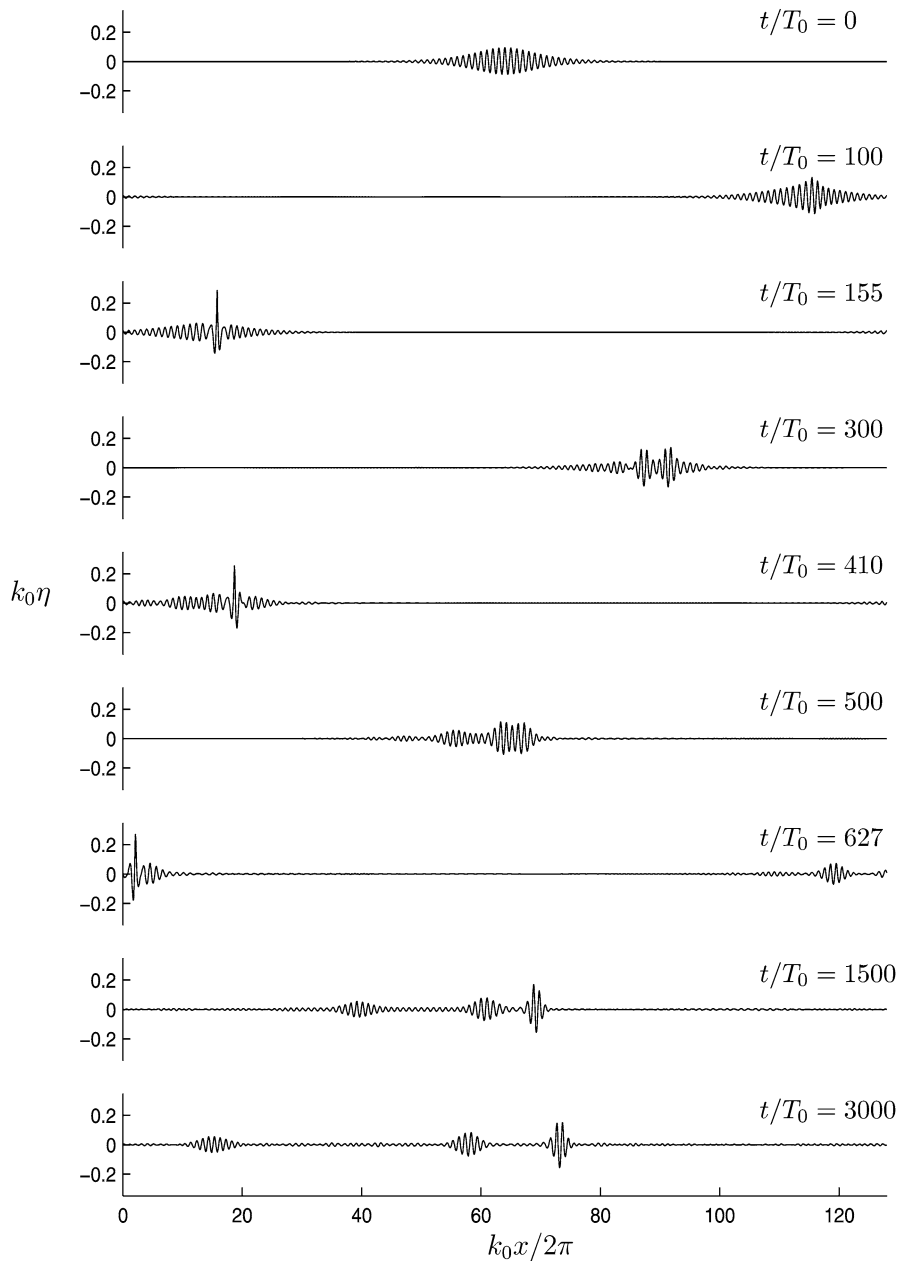


Fig. 1. Evolution of the free surface. Fully nonlinear simulation (CG model).

validity (few tens of wave periods), the number of observed solitons is in good agreement with the predictions based on the inverse scattering technique for NLS.

From a qualitative point of view, a somewhat better agreement is obtained with the EDE model. This model predicts rather well the early stages of the group splitting (up to  $t/T_0 = 300$ ) and the characteristic features of the evolution, namely the separation into solitary wave groups and temporary downshifting. However, the EDE model fails to predict the long-time scenario based on the CG predictions. Indeed, the EDE model predicts the formation of rank-ordered solitary wave groups. The larger, the faster to separate and propagate ahead of the group of waves. Once formed, it evolves independently of the other part of the group. In the trailing part, the computations with the EDE show weak and slow interactions between the two other solitons that are forming. These two solitons in the trail remain “attached” for a much longer time than predicted by the fully nonlinear scenario. In contrast, the CG model predicts

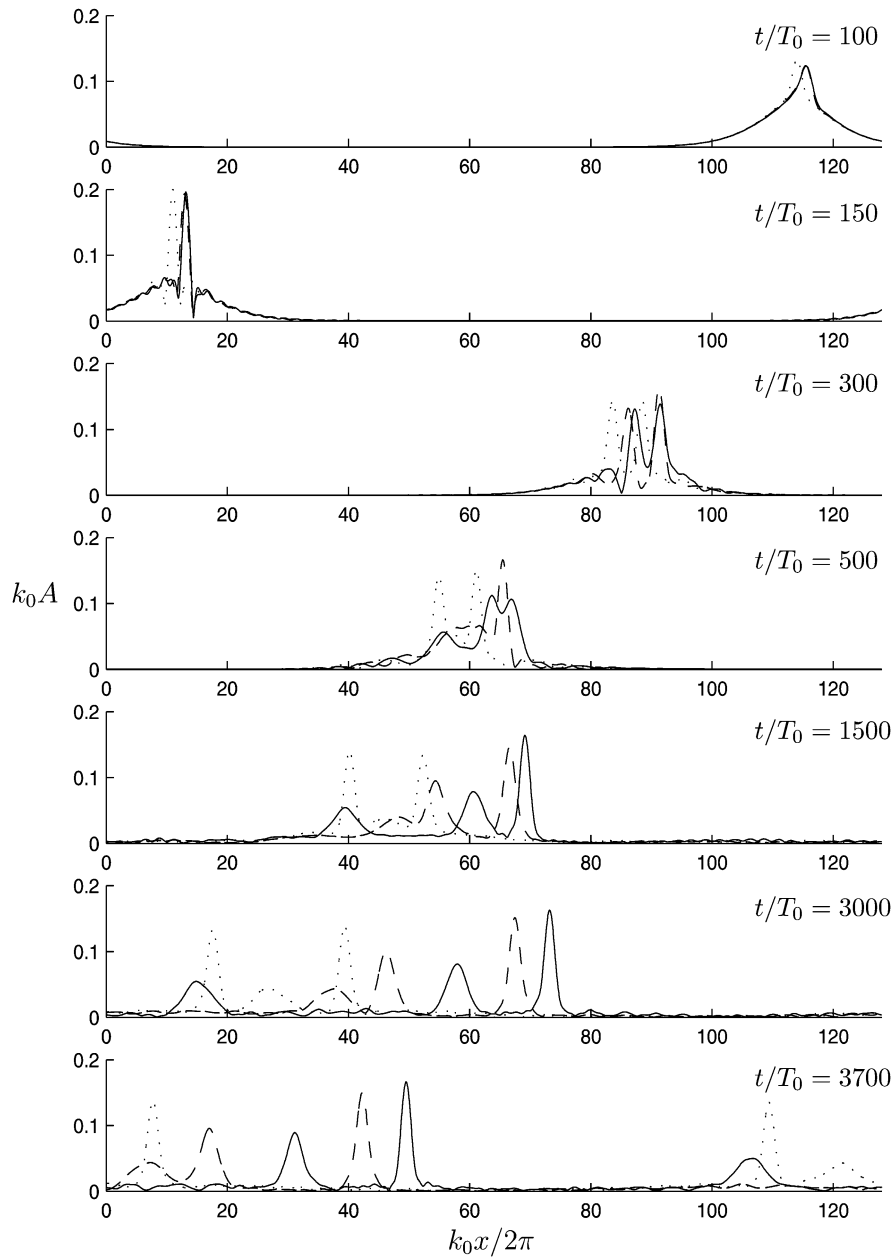


Fig. 2. Envelope of the surface. (—) CG, (---) EDE, (···) NLS.

a much more complicated scenario, with stronger interactions between the forming solitary waves. This is illustrated by the formation of two supplementary extreme wave events before separation occurs.

The differences between the EDE model and the fully nonlinear CG model suggest that the long-time evolution of the wave group is driven by higher-order nonlinear effects that are not captured by the EDE model. This may also be related to the narrow-band assumption still embedded in the derivation of the EDE model. After the first demodulation phase ( $t/T_0 \geq 300$ ), there is a significant broadening of the wave elevation spectrum. This, in turn, can affect the validity and accuracy of the EDE. Nevertheless, this extension of Dysthe's equation describes rather well the first asymmetric modulations of the group envelope (contrary to NLS) as well as the increase of the speed of propagation of the strong modulation developing in the central part of the group in comparison with NLS. Thus, it

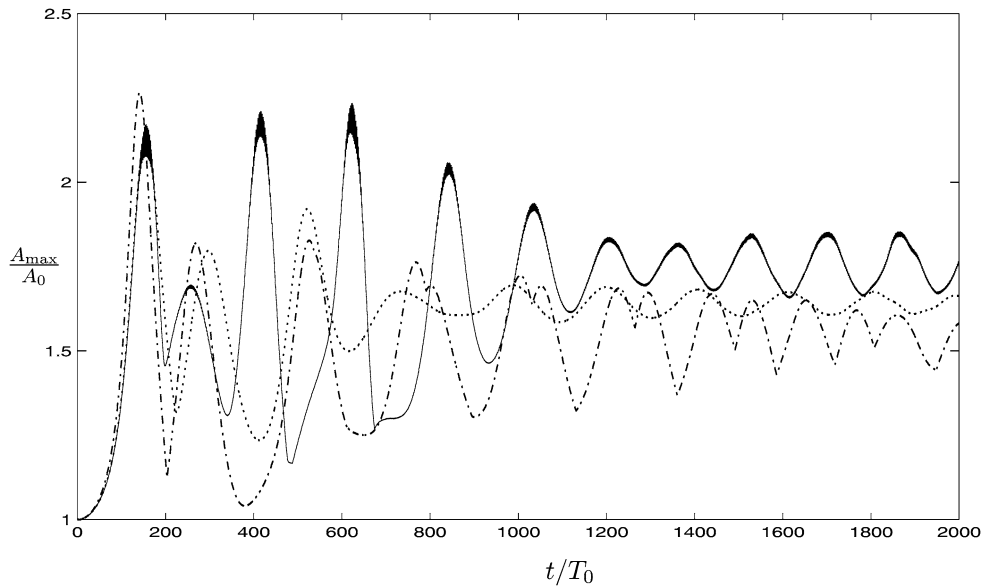


Fig. 3. Temporal evolution of the amplification factor. (—) CG, (···) EDE, (---) NLS.

may be worthwhile to develop a generalization of the EDE, including higher (quintic) nonlinear terms to improve the accuracy and the time range of validity of EDE, when nonlinear dispersive focusing in long wave groups is considered.

Fig. 3 shows the time evolution of the amplification factor of the amplitude of the complex envelope, i.e.  $A_f = \max_x(|A(x, t)|)/\max_x(|A(x, 0)|)$ , obtained with the CG model and the weakly nonlinear models for narrow-banded waves. According to the fully nonlinear predictions, the first soliton has detached from the other waves for  $t/T_0 \geq 1200$ . Thus from this time, the computed normalized maximal envelope amplitude of the wave field corresponds to the maximal envelope amplitude of the highest solitary wave group. It is observed that the normalized maximal envelope amplitude oscillates about the value 1.75 with a period of approximately 170 fundamental wave periods.

### 3.2. Comparison with HOSM

Fig. 4 demonstrates that the computations based on HOSM support the predictions of the CG model. We have found the HOSM with  $M \geq 3$  is in good agreement with the CG model. When we increase the nonlinear parameter  $M$  in the HOSM from  $M = 3$ , the agreement is improved and, this, for a larger time range up to  $t/T_0 \approx 1000$ .

As expected, the HOSM with  $M = 3$  is largely superior to the EDE model since it is free of any-bandwidth constraint. In principle, the HOSM with  $M = 3$  is an extension of the third-order Zakharov equations. Since it is free of any bandwidth restriction like the Zakharov equation and is accurate to the third-order in the wave steepness, it does a fairly good job in predicting the long-time evolution of the wave group.

It is important to mention here that, first, we had used the formulation as proposed by Dommermuth and Yue [24] that differs from the formulation used in this paper as explained above (see Section 2.2). Surprisingly, it was found that this formulation of HOSM with  $M = 3$  and  $M = 4$  is worse than the EDE model, as far as the long-time scenario of the wave group evolution is concerned. Indeed, although these HOSM predictions are in better agreement with the CG model for the first freak wave event near  $t/T_0 \approx 155$  and even later up to  $t/T_0 \leq 300$ , it fails to predict the separation of the two leading solitons. These two solitons interact as a bound-solitons state. This recurring interaction corresponds to the quasi-periodic formation of freak waves events. These results are not shown here. When we had increased the order parameter  $M > 4$  in the formulation of Dommermuth and Yue [24], after having checked the numerical implementation, we observed a substantial and systematic improvement with regards to the results from West et al.'s formulation and, thus, the CG predictions. Therefore, it is found that the inconsistency of the HOSM formulation of Dommermuth and Yue is critical, unless  $M > 4$ , to study the long-time evolution of nonlinear wave

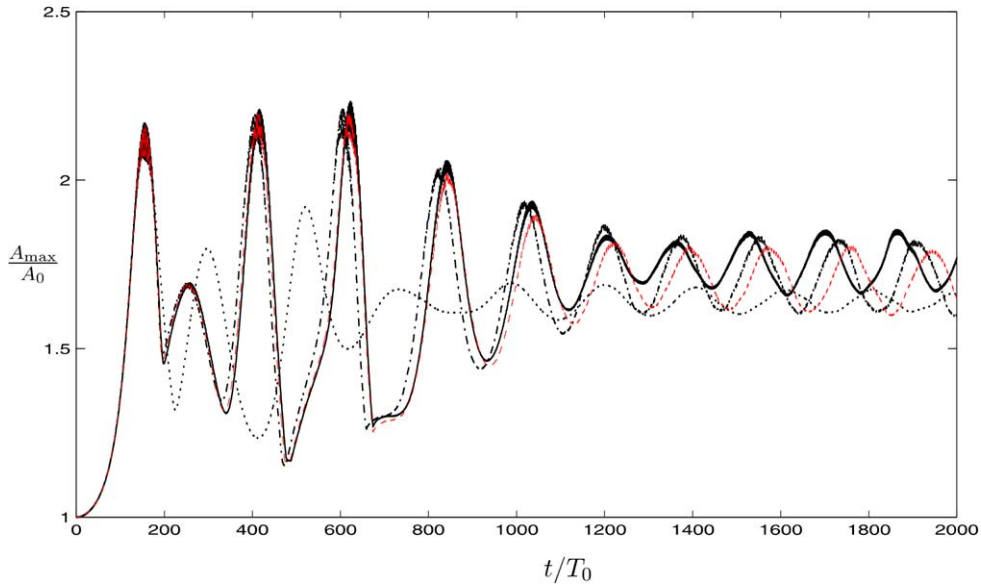


Fig. 4. Temporal evolution of the amplification factor. (—) CG, (– –) HOSM with  $M = 4$ , (– · –) HOSM with  $M = 3$ , (···) EDE.

groups as considered in this paper. In contrast, the formulation of the HOSM based on the approach of West et al. [3] appears to be superior when  $M = 3$  and  $M = 4$ .

We note also that we have used different time integrators for the CG model and the HOSM. Thus, the accumulation of phase-lags and round-off errors in the HOSM result in slight differences in the long term as compared to the CG results. After the complete separation of the three solitary envelopes, the differences between the CG model and HOSM are essentially in the relative positions of the solitary wave groups. It should be noted that the frequency cut-off  $k_{\max}$  does not alter significantly the good agreement with the CG results during the splitting process, provided it is sufficiently large. We have chosen  $k_{\max} = 960$  for  $M = 3$  and  $M = 4$ , so that the HOSM always resolve up to the eight harmonics of the carrier wave without aliasing errors.

#### 4. Formation of large wave events

The nonlinear evolution of the wave group near the formation of the first freak wave is illustrated here by the Fourier transform  $|\mathcal{F}\{\eta_x\}|$  of the surface slope  $\eta_x$  (see Fig. 5). The initially narrow spectrum widens during the evolution of the group. Fig. 5 shows that growth of side-bands is an inherent feature in the formation of the first large wave event taking place at time  $t/T_0 = 155$ . The spectrum is characterized by substantial transfer of energy to sub- and super-harmonic wavenumbers. The energy content at the central wavenumber is reduced accordingly.

The role of the super-harmonic wavenumbers during the first large wave event is highlighted by the Fourier spectrum of the wave elevation at times  $t/T_0 = 155, 156, 157, 158$  (see Fig. 6). The pronounced tail at high wavenumbers exhibits an oscillatory appearance with period  $2T_0$ . This oscillation enhances the (tall) wave elevation for  $t/T_0 = 155, 157$  and reduces the (deep) trough for  $t/T_0 = 156, 158$  occurring during the large wave event. The transfer of energy to the high wavenumbers takes place during only a short period of time. The computations show that the dominant side-bands peak at wavenumbers  $k_1 = 0.93k_0$  and  $k_2 = 1.14k_0$  when the first large event occurs, a result that is also obtained using EDE. Other runs with different initial steepness indicate that the dominant side-bands of the Fourier spectrum recur with a time scale proportional to  $(a_0k_0)^{-2}$ . The results of these runs are not reported here. For the present experiment, we note that the most unstable side bands appear at symmetric wavenumbers with  $\Delta k/k_0 = 2a_0k_0 = 0.18$ . This is observed in the initial part of the simulations using the fully nonlinear scheme, EDE and NLS equations. The latter equation predicts side bands at symmetric satellites with  $\Delta k/k_0 = 2a_0k_0 \simeq 0.15$  when the nonlinearity is appreciable (see Fig. 7).

For the integrable NLS equation, it is well-known that there is a close relation between the side-band instabilities of a plane wave and breather type solutions (homoclinic orbits). As demonstrated in [31], these homoclinic orbits

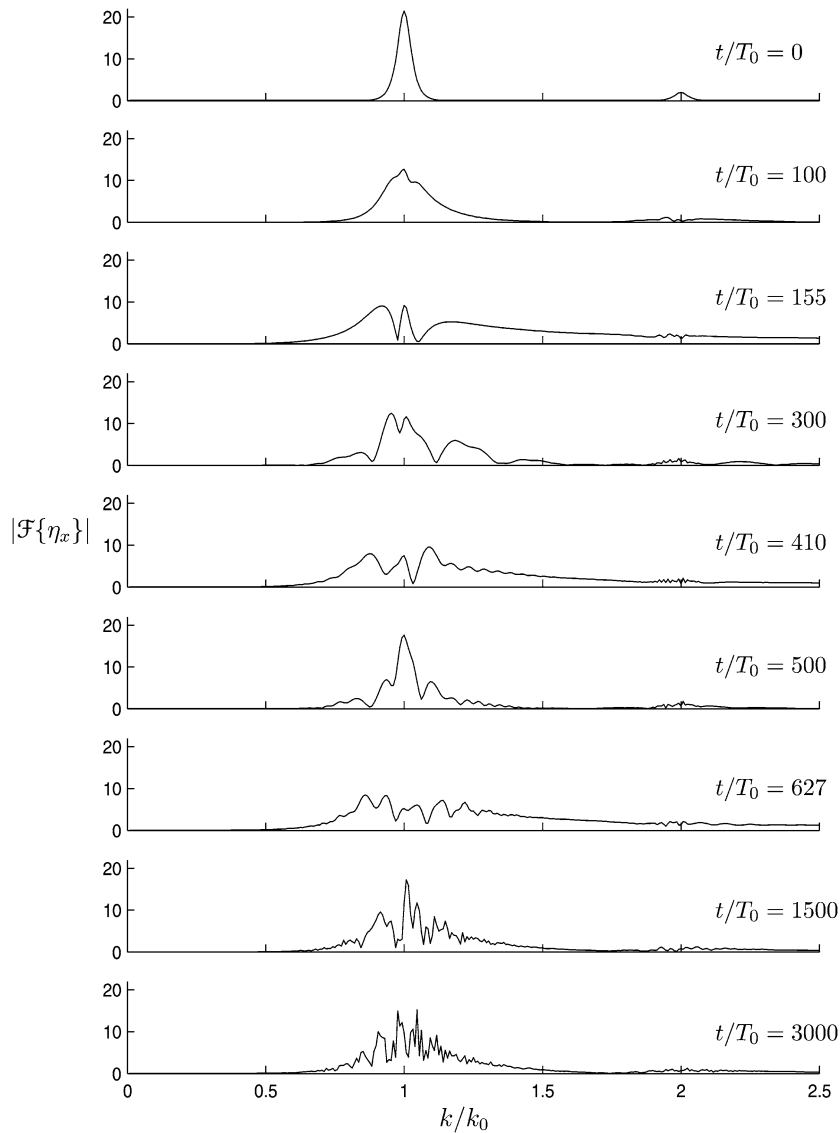


Fig. 5. Spectrum of the surface slope. Fully nonlinear simulation corresponding to Fig. 1.

are associated with each unstable modes of the unperturbed plane wave, and play a significant role in the long time evolution of a perturbed plane wave. Using perturbed NLS equations, the authors conjectured that the generation of freak waves is related to the persistence of NLS homoclinic structures in the higher-order nonlinear models. Given that the first stage of our numerical simulation is characterized by strong side-band instabilities, it is tempting to compare the first large wave event with an analytical breather type solution of NLS equation. Nevertheless, it should be recognized that our initial value problem is rather different from that where the initial state is a periodically, weakly modulated plane wave.

It would seem natural to compare our first large wave event with the space-periodic Akhmediev's breather solution, as underlined in [9], given that we have used periodic boundary conditions. Nevertheless, this is hardly possible here since there is no clear space-periodicity in the amplitude envelope at the first maximum modulation near  $t/T_0 = 155$ . Thus, we have preferred to compare the first wave event with the time-periodic solution found by Ma [32]. If we use the transformation

$$X = 2k_0(x - c_g t), \quad T = \frac{1}{2}\omega_0 t, \quad q = 2^{-1/2}k_0 A^*, \quad (11)$$

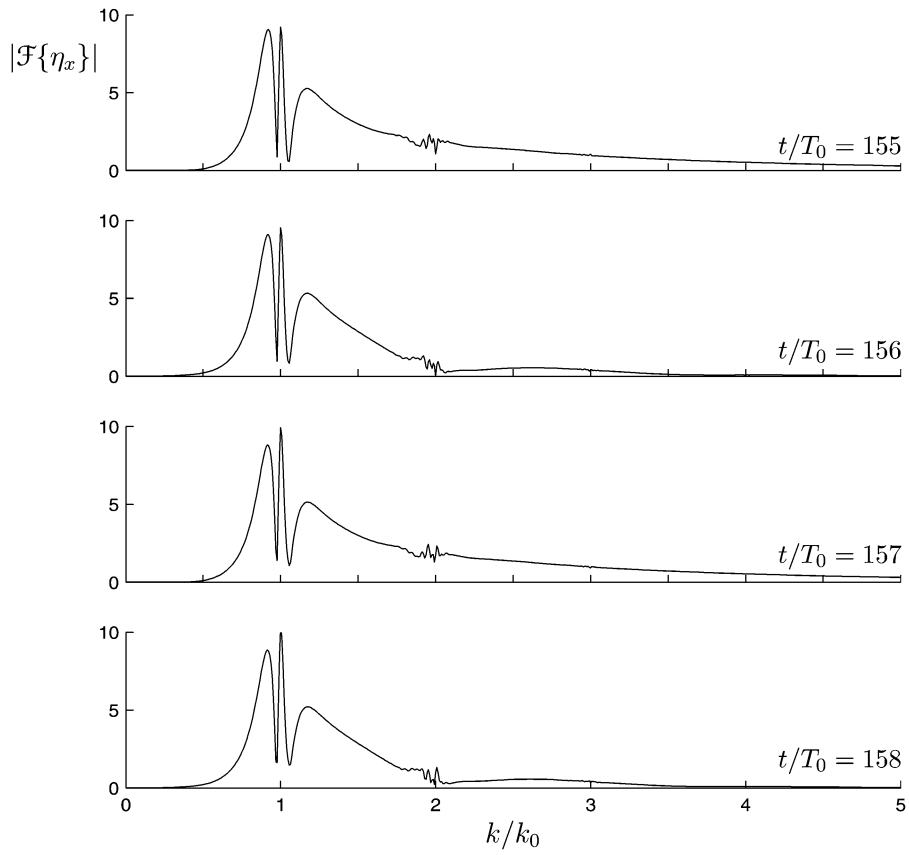


Fig. 6. Transfer of energy in the spectrum of the surface slope (CG model).

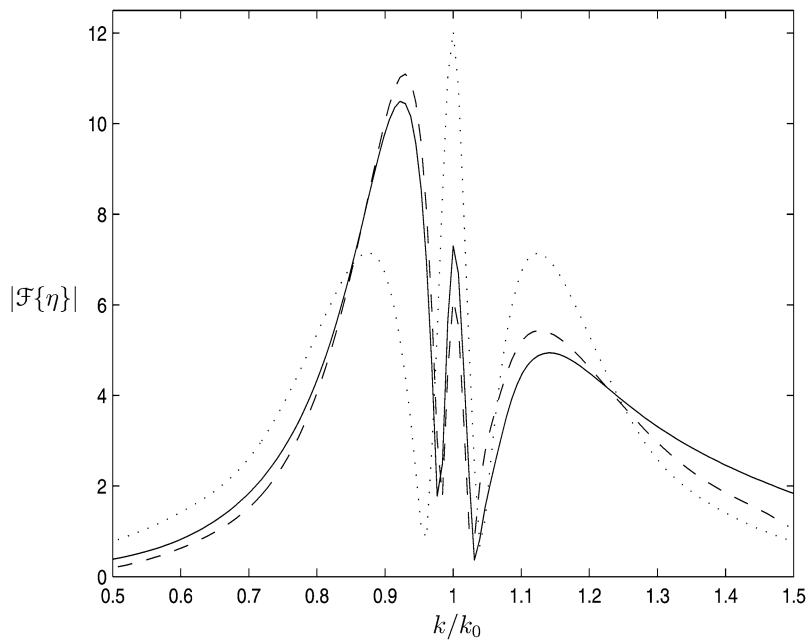


Fig. 7. Fourier spectrum of the wave surface at  $t/T_0 = 155$ . (—) CG, (---) EDE, (···) NLS.

then the cubic NLS equation (8) can be written in a canonical form as

$$iq_T + q_{XX} + 2|q|^2q = 0. \quad (12)$$

The *Ma-breather* solution is periodic in time and tends to the plane wave solution as  $X$  goes to  $\pm\infty$ . The canonical expression of the *Ma-breather* solution is

$$q(X, T) = e^{2iT} \frac{\cos(\Omega T - 2i\phi) - \cosh(\phi) \cosh(pX)}{\cos(\Omega T) - \cosh(\phi) \cosh(pX)}, \quad (13)$$

which is a one-parameter solution depending on  $\phi$  with the following relations

$$\Omega = 2 \sinh(2\phi), \quad p = 2 \sinh(\phi), \quad |q_{\max}| = 1 + 2 \cosh(\phi). \quad (14)$$

We scaled out this solution with steepness  $\varepsilon_0 = a_0 k_0$  as

$$A(x, t) = a_0 e^{\frac{i}{2}\varepsilon_0^2\omega_0 t} \frac{\cos(\frac{1}{4}\Omega\varepsilon_0^2\omega_0 t - 2i\phi) - \cosh(\phi) \cosh[p\sqrt{2}\varepsilon_0 k_0(x - c_g t)]}{\cos(\frac{1}{4}\Omega\varepsilon_0^2\omega_0 t) - \cosh(\phi) \cosh[p\sqrt{2}\varepsilon_0 k_0(x - c_g t)]}. \quad (15)$$

The envelope of this solution oscillates in time while it propagates with the linear group velocity of the carrier wave. In order to test the first large wave event we have fitted the *Ma-breather* solution, with  $T = 0$  in Eq. (13), so that its maximum amplitude equals to the maximum amplitude of the envelope of the CG numerical solution at  $t/T_0 = 155$ . The parameter  $\phi$  is then determined with the equation

$$|q_{\max}| = 1 + 2 \cosh(\phi) = \max(|A|)/a_0. \quad (16)$$

The best comparison is obtained when we take the initial amplitude to be  $a_0 = 0.062$  for which  $\phi \approx 1.22$ . Fig. 8 shows the comparison of the CG solution with the propagating *Ma-breather* for  $t/T_0 = 155, 156, 157$  and  $158$ . The *Ma-breather* may seem quite close to the numerical solution only in the central part of the wave group and on the rear face of the modulation. Although the simulated envelope presents locally some similarity with the *Ma-breather*, the wave elevation differs considerably from that of *Ma's* solution. In particular, the structure and the number of waves on the two sides of the center of the modulation are markedly different. Besides, the propagation velocity of the numerical envelope is greater than that of the *Ma breather* solution, i.e. the linear group velocity of the perturbed plane wave.

Looking at the shape of the wave group, Fig. 9(a)–(c) show that the first large wave event is accurately described by HOSM ( $M \geq 3$ ) solutions, while the NLS and EDE predictions are less impressive. Nevertheless, the EDE is in considerably better agreement than NLS with the higher-order nonlinear computations to describe the formation of the first freak wave. As mentioned in Section 3.1, the two other large wave events observed with the fully nonlinear models are not predicted by NLS and EDE models. Looking at the evolution of the wave group envelope reveals that these two large wave events should rather be interpreted as nonlinear collisions between pairs of solitary wave groups (see Figs. 1 and 2).

It may be of interest, here, to point out that there exists generalized *Ma-breather* solutions that can propagate at a velocity greater than the linear group velocity of the carrier wave. This solution describes breathing solitary waves on a background plane wave. It includes the *Ma-breather*, the Akhmediev and the Peregrine solutions as particular cases. The characteristics of these solutions have been used in [33] for the analysis of envelope soliton interactions and their detection in freak waves time records. Thus, it would be interesting to use this approach based on the inverse scattering technique, in order to analyze our results and to get more insights in the observed nonlinear interactions of the group of waves during the split-up.

## 5. Multiple collision of envelope solitons

Earlier experiments in a long wave tank demonstrated several interesting features of group splitting in deep water. In [13], the evolution of wave packets initially with a rectangular shaped envelope has been investigated by varying the length of the packets (number of wave in the initial packet) and the initial wave slope in the range 0.09–0.28. For wave groups of sufficiently large initial steepness, an interesting feature of the group splitting process is the frequency downshift in the leading groups which has been reported. For short wave groups and sufficiently large steepness ( $ak \geq 0.15$ ), the wave packets generally exhibited a permanent frequency downshift. Not all of the groups were downshifted. Besides, it has been reported for long wave groups that very strong asymmetric modulations occur

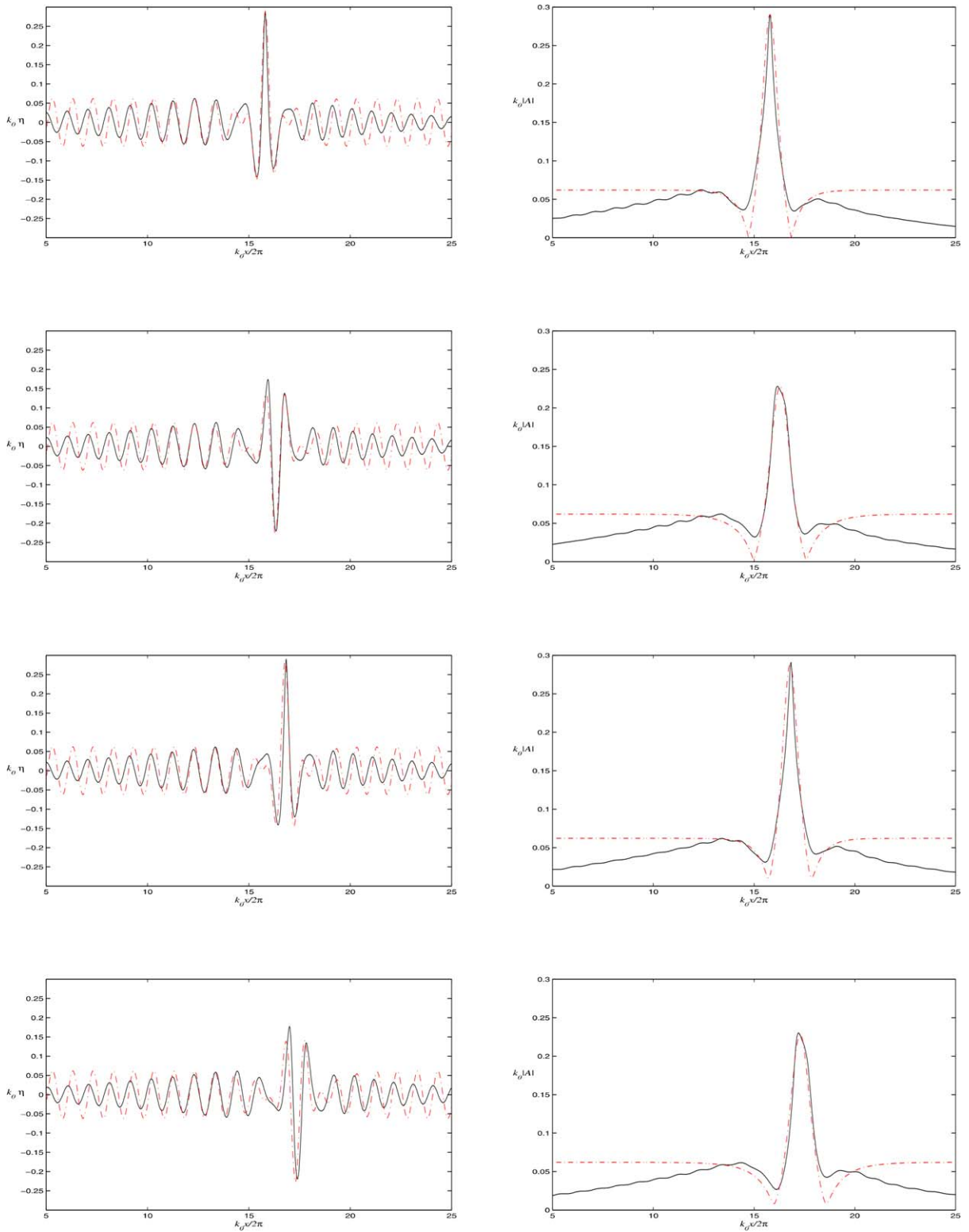


Fig. 8. Elevation (left) and envelope (right) of the surface elevation at  $t/T_0 = 155, 156, 157, 158$ . (—) CG solution, (---) fitted analytical Ma-breather solution.

in the central part of the wave group in contrast with the evolution of long wave groups of small initial steepness ( $ak < 0.10$ ). These strong modulations were associated with strong interactions of solitons with different carrier frequency (or wavenumber) that are in different evolutionary stages. These collisions of envelope occur because envelope solitons with lower carrier wavenumber propagates faster and, consequently, run into the leading solitons with a higher carrier wavenumber. When this phenomenon occurs, wave breaking is systematically observed.

Our numerical simulations show that collisions of envelope solitons can occur in the transformation of a long wave group with an initial symmetric shape even though the initial steepness is small (here  $a_0k_0 = 0.09$ ). While a permanent downshifting in the leading groups is observed experimentally for the initially steeper waves, namely  $ak \geq 0.15$  in [13], our numerical simulations show only a temporary downshifting in wavenumber. This occurs during the formation of the large wave events. This temporary downshifting is associated with the temporary excitation of side-band modes in the spectrum, the subharmonic modes containing more energy (when a freak wave occurs) than their symmetric counterparts. The dominant character of certain subharmonic modes over other side-band modes is evidenced in the physical space by a slight increase in the wavelength on both sides of the maximal elevation of the freak waves. Other numerical simulations of long wave groups with initial steepness as small as  $a_0k_0 = 0.046$  (results not shown here) show that the same temporary downshifting of the spectrum occurs and is associated with the occurrence large wave events.

While we find here that the subharmonic contribution is temporary, a permanent downshifting in two-dimensional flows is known to be related with non-conservative effects, such as breaking or generation of capillary waves [34]. A different cause of downshift, that is independent of dissipation (and breaking), was explained theoretically by Trulsen and Dysthe [35] and confirmed experimentally [36]. They showed that evolution of Stokes waves can lead to significant growth of standing waves across the tank. This three-dimensional mechanism is responsible for transfer of energy from the long crested wave mode to lateral modes. The process is irreversible and is characterized by an energy transfer to both higher and lower wavenumbers. The dominant wavenumber is always downshifted. Three-dimensional downshifting is observed in wave tanks when the ratio  $\Delta\mu = k_{\text{lateral}}/k_0$  is less than about 0.1, where  $k_{\text{lateral}} = \pi/b$  denotes the smallest lateral vector component in a wavetank of width  $b$  and  $k_0$  is the wavenumber of deep water Stokes waves. Experimental  $\Delta\mu$ -values are 0.066 [5], 0.125 [13], 0.074 [36]. It is evident that the permanent downshift observed in the experiments by Su [13] involves a combination of three-dimensional nonlinear modulation, dissipation and wave breaking (no obvious explanation of the permanent downshift was given in his paper).

Finally, we note that it is well known that transverse instabilities of solitary waves have been predicted theoretically almost 30 years ago for the solution of NLS equation [37]. Therefore, it would be interesting to investigate numerically the impact of three-dimensional perturbations on the long time evolution and, in particular, on the solitary waves collisions that we have studied in this work.

## 6. Conclusion

The main focus of the present paper has been to support the predictions obtained in [19] with the CG model. To do this, we have employed a high-order spectral method (HOSM) slightly different than that proposed by West et al. [3] and Dommermuth and Yue [24]. For the simulation considered in this paper, the splitting process happens on time-scales beyond the time range of validity of the simplified model equations like NLS equation and EDE equations [2]. Hence, these simplified models fail to describe the freak wave events due to collision of pairs of envelope solitons, and which occur out of the time range of validity of both weakly nonlinear models. Nevertheless, one can observe that the EDE model simulate quite well the formation of the first freak wave in comparison with the NLS equation.

In contrast with the weakly nonlinear models for narrow-banded waves, it is remarkable that both the CG model and HOSM predict not only a different long-time scenario but also a larger number of freak wave events during the group splitting. These fully nonlinear computations predict at the end of the group splitting a train of three height-ordered solitary wave groups, the larger ahead of the others and each having the same carrier wavenumber as that of the initial wave group.

For the long-time simulations considered in this paper, a good agreement is found between the CG model and both formulations of HOSM provided  $M > 4$ . However, an important issue concerning the representation and the treatment of the vertical velocity in the HOSM formulation is highlighted here. In particular, the West et al. formulation of the HOSM (for  $M = 3$  and  $M = 4$ ) is found to be much superior in predicting the long-time evolution, as compared to

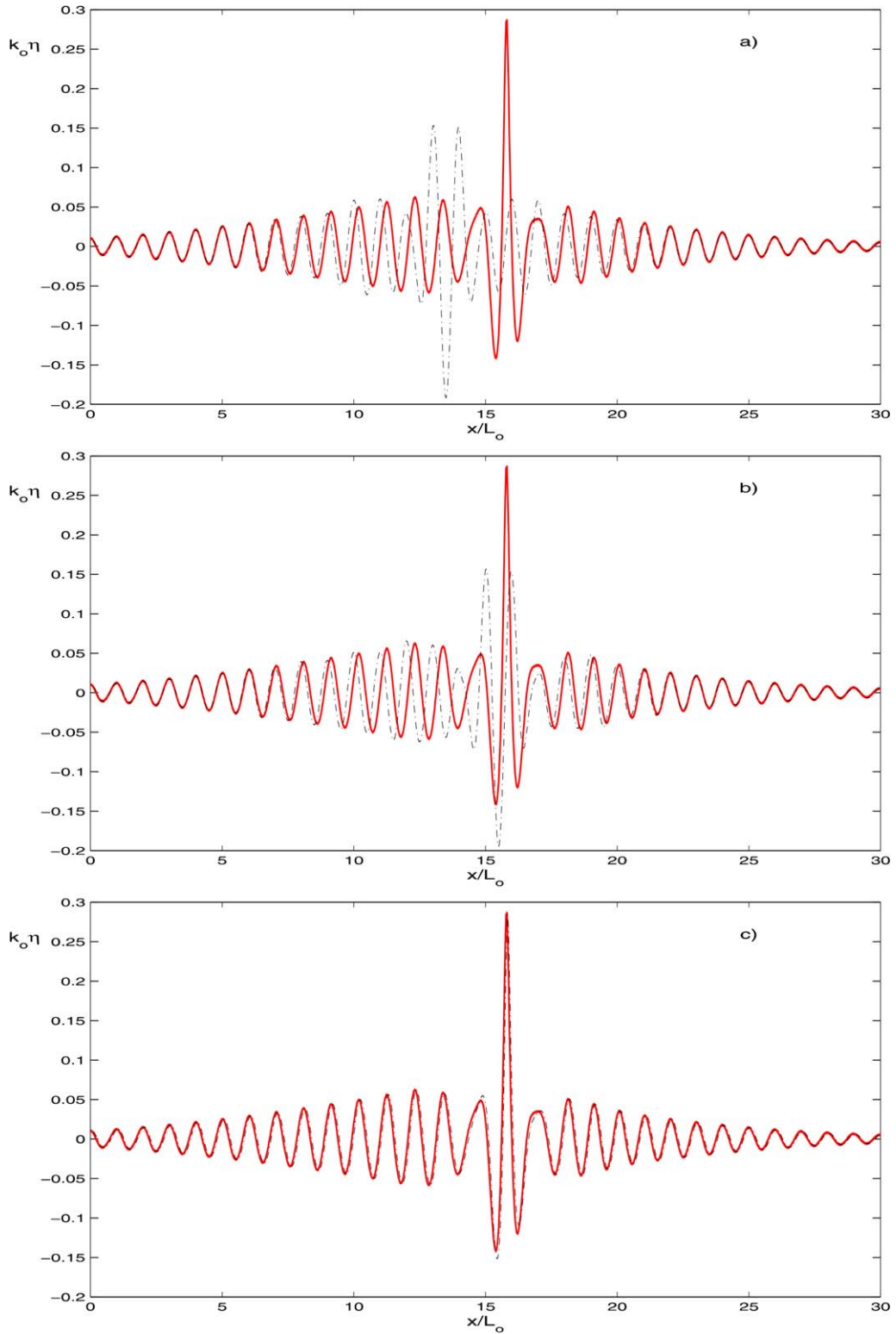


Fig. 9. Comparison of surface elevations at  $t/T_0 = 155$  between CG solution (solid line) and (a) NLS (dash-dot line); (b) Dysthe (dash-dot line); (c)  $M = 4$  (dash-dot line).

the formulation of Dommermuth and Yue that is inaccurate in the long term of our numerical simulations. To the authors' knowledge these quantitative differences between these two HOSM formulations has not been documented in previous studies.

These numerical results also demonstrate that the formation of the large wave events can occur during the transformation of a long wave group even if the steepness is initially small. During the transition to a stable state of several solitary wave groups, strong nonlinear effects lead to the formation of three large wave events. These strong nonlinear effects are seen here as strong interactions or collisions of three solitary wave groups on a background of dispersive wave packets, which form at different time and position in the evolving group of waves.

The role of sideband instabilities and temporary downshifting has been highlighted here. We observe that large wave events occur when side-band modes of the carrier wavenumber reach maximum amplitudes during the evolution. The greater amplification of certain subharmonic side-band modes results in a temporary downshifting of the peak of the wave spectrum. We note that the permanent downshift in the leading groups observed in the experiments by Su [13] when  $ak \geq 0.15$  were caused by a combination of nonconservative effects (dissipation and wave breaking) and conservative effects (transfer of wave energy to lateral standing wave modes, the latter explained in Section 5). Such a permanent downshift cannot be obtained from the two-dimensional conservative equations employed in the present study. Moreover, the existence of transverse three-dimensional instabilities of the NLS solitary wave solutions suggests that the long time evolution may be influenced by these effects. This is a topic for future research.

## Acknowledgements

The present authors are grateful to the reviewers of this paper for their valuable comments and suggestions, which have helped us to improve the presentation of this work.

D. Clamond and J. Grue were supported by the Research Council of Norway through the Strategic University Program (Contract No. NFR 146526/420): "Modelling of currents and waves for sea structures" at the University of Oslo.

## References

- [1] D. Clamond, J. Grue, A fast method for fully nonlinear water wave computations, *J. Fluid Mech.* 447 (2001) 337–355.
- [2] K. Trulsen, I. Kliakhandler, K.B. Dysthe, M.G. Velarde, On weakly nonlinear modulation of waves on deep water, *Phys. Fluids* 12 (10) (2000) 2432–2437.
- [3] B.J. West, K.A. Brueckner, R.S. Janda, A method of studying nonlinear random field of surface gravity waves by direct numerical simulation, *J. Geophys. Res.* 92 (C11) (1987) 11 803–11 824.
- [4] C. Kharif, E. Pelinovsky, Physical mechanisms of the rogue wave phenomenon, *Eur. J. Mech. B Fluids* 22 (2003) 603–634.
- [5] B.M. Lake, H.C. Yuen, H. Rungaldier, W.E. Ferguson, Nonlinear deep-water waves. Theory and experiment. Evolution of a continuous wave train, *J. Fluid Mech.* 83 (1977) 49–74.
- [6] W.K. Melville, The instability and breaking of deep-water waves, *J. Fluid Mech.* 115 (1982) 165–185.
- [7] H.C. Yuen, B.M. Lake, Nonlinear dynamics of deep-water gravity waves, *Adv. Appl. Mech.* 22 (1982) 67–229.
- [8] K.L. Henderson, D.H. Peregrine, J.W. Dold, Unsteady water wave modulations: fully nonlinear solutions and comparison with the nonlinear Schrödinger equation, *Wave Motion* 29 (1999) 341–361.
- [9] K.B. Dysthe, K. Trulsen, Note on breather type solutions of the NLS as models for freak-waves, *Phys. Scripta* 82 (1999) 48–52.
- [10] A.R. Osborne, M. Onorato, M. Serio, The nonlinear dynamics of rogue waves and holes in deep-water gravity wave train, *Phys. Lett. A* 275 (2000) 386–393.
- [11] K. Kharif, E. Pelinovsky, T. Talipova, A. Slunyaev, Focusing on nonlinear wave groups in deep water, *JETP Lett.* 73 (4) (2001) 170–175.
- [12] V.E. Zakharov, A.B. Shabat, Exact theory of two-dimensional self-focusing and one-dimensional self-modulation of waves in nonlinear media, *Sov. Phys. JETP* 34 (1972) 62–69 (English translation).
- [13] M.Y. Su, Evolution of groups of gravity waves with moderate to high steepness, *Phys. Fluids* 25 (12) (1982) 2167–2174.
- [14] T.K. Chereskin, E. Mollo-Christensen, Modulational development of nonlinear gravity-wave groups, *J. Fluid Mech.* 151 (1985) 337–365.
- [15] E. Lo, C.C. Mei, A numerical study of water-wave modulation based on a higher-order nonlinear Schrödinger equation, *J. Fluid Mech.* 150 (1985) 385–416.
- [16] K.B. Dysthe, Note on a modification to the nonlinear Schrödinger equation for application to deep water, *Proc. Roy. Soc. London A* 369 (1979) 105–114.
- [17] L. Shemer, E. Kit, H. Jiao, An experimental and numerical study of the spatial evolution of unidirectional nonlinear water-wave groups, *Phys. Fluids* 14 (2002) 3380–3390.
- [18] L. Shemer, H. Jiao, E. Kit, Y. Agnon, Evolution of a nonlinear wave field along a tank: experiments and numerical simulations based on the spatial Zakharov equation, *J. Fluid Mech.* 427 (2001) 107–129.

- [19] D. Clamond, J. Grue, Interaction between envelope solitons as a model for freak wave formations. Part I: Long time interaction, *C. R. Acad. Sci.* 330 (8) (2002) 575–580.
- [20] D. Fructus, D. Clamond, J. Grue, Ø. Kristiansen, An efficient model for three-dimensional surface wave simulations. Part I: Free space problems, *J. Comp. Phys.* 205 (2) (2005) 665–685.
- [21] D. Clamond, D. Fructus, J. Grue, Ø. Kristiansen, An efficient model for three-dimensional surface wave simulations. Part II: Generation and absorption, *J. Comput. Phys.* 205 (2) (2005) 686–705.
- [22] D. Fructus, C. Kharif, M. Francius, Ø. Kristiansen, D. Clamond, J. Grue, Dynamics of crescent water wave patterns, *J. Fluid Mech.* 537 (2004) 155–186.
- [23] Ø. Kristiansen, D. Fructus, D. Clamond, J. Grue, Simulations of crescent wave patterns on finite depth, *Phys. Fluids* 17 (2005) 064101.
- [24] D. Dommermuth, D.K.P. Yue, A high-order spectral method for the study of nonlinear gravity waves, *J. Fluid Mech.* 184 (1987) 267–288.
- [25] M. Tanaka, A method of studying nonlinear random field of surface gravity waves by direct numerical simulation, *Fluid Dyn. Res.* 28 (2001) 41–60.
- [26] C. Skandrani, C. Kharif, J. Poitevin, Nonlinear evolution of water surface waves: the frequency down-shift phenomenon, *Contemp. Math.* 200 (1996) 157–171.
- [27] K. Trulsen, K.B. Dysthe, A modified nonlinear Schrödinger equation for broader bandwidth gravity waves on deep water, *Wave Motion* 24 (1996) 281–289.
- [28] M. Stiassnie, L. Shemer, On modifications of the Zakharov equation for surface gravity waves, *J. Fluid Mech.* 143 (1984) 47–67.
- [29] J.D. Fenton, The numerical solution of steady water wave problems, *Computers & Geosciences* 14 (3) (1988) 357–368.
- [30] A.I. Dyachenko, V.E. Zakharov, Modulational instability of Stokes waves  $\rightarrow$  freak waves, *JETP Lett.* 81 (6) (2005) 255–259.
- [31] A. Calini, C.M. Schober, Homoclinic chaos increases the likelihood of rogue wave formation, *Phys. Lett. A* 298 (2002) 335–349.
- [32] Y.-Ch. Ma, The perturbed plane-wave solutions of the cubic Schrödinger equation, *Stud. Appl. Math.* 60 (1979) 43–58.
- [33] A. Slunyaev, Nonlinear analysis and simulations of measured freak wave time series, *Eur. J. Mech. B Fluids* 25 (5) (2006) 621–635.
- [34] F. Dias, C. Kharif, Nonlinear gravity and capillary-gravity waves, *Annu. Rev. Fluid Mech.* 31 (1999) 301–346.
- [35] K. Trulsen, K. Dysthe, Frequency downshift in three-dimensional wave trains in a deep basin, *J. Fluid Mech.* 352 (1997) 359–373.
- [36] K. Trulsen, C.T. Stansberg, M.G. Velarde, Laboratory evidence of three-dimensional frequency downshift of waves in a long tank, *Phys. Fluids* 11 (1) (1999) 235–237.
- [37] V.E. Zakharov, A.M. Rubenchik, Instability of waveguides and solitons in nonlinear media, *Sov. Phys. JETP* 38 (1974) 494–500.